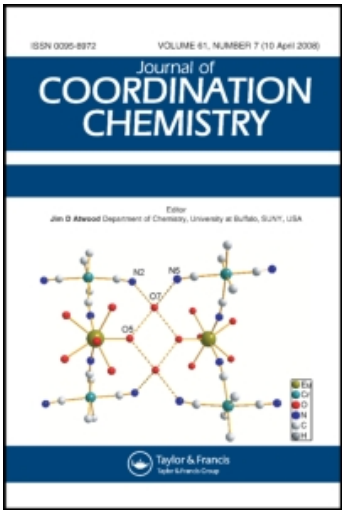

Journal of Coordination Chemistry
Publication details, including instructions for authors and subscription information:
http://www.informaworld.com/smpp/title~content=t713455674

Solubility measurements of crystalline β-$Ni(OH)_2$ in aqueous solution as a function of temperature and pH

Donald A. Palmer[a]; Heinz Gamsjäger[b]
[a] Chemical Sciences Division, Oak Ridge National Laboratory, Oak Ridge, TN 37831-6110, USA [b] Lehrstuhl für Physikalische Chemie, Montanuniversität Leoben, Austria

First published on: 14 June 2010

To cite this Article Palmer, Donald A. and Gamsjäger, Heinz(2010) 'Solubility measurements of crystalline β-$Ni(OH)_2$ in aqueous solution as a function of temperature and pH', Journal of Coordination Chemistry, 63: 14, 2888 — 2908, First published on: 14 June 2010 (iFirst)
To link to this Article: DOI: 10.1080/00958972.2010.492215
URL: http://dx.doi.org/10.1080/00958972.2010.492215

Journal of Coordination Chemistry
Vol. 63, Nos. 14–16, 20 July–20 August 2010, 2888–2908

Solubility measurements of crystalline β-Ni(OH)$_2$ in aqueous solution as a function of temperature and pH

DONALD A. PALMER*† and HEINZ GAMSJÄGER‡

†Chemical Sciences Division, Oak Ridge National Laboratory, PO Box 2008, Oak Ridge, TN 37831-6110, USA
‡Lehrstuhl fűr Physikalische Chemie, Montanuniversität Leoben, A-7800 Leoben, Austria

(*Received 18 January 2010; in final form 11 March 2010*)

Experimental results on the solubility of crystalline nickel hydroxide (theophrastite), according to the dissolution reaction, β-Ni(OH)$_2$(cr) + 2H$^+$ $\rightleftarrows$ Ni^{2+} + 2H$_2$O(l), are reported as functions of temperature (0–200°C) and pH at pressures slightly exceeding saturation vapor pressure. The experiments were carried out in either various flow-through cells or a hydrogen-electrode concentration cell (HECC). The results were treated with a thermodynamic model incorporating only the unhydrolyzed aqueous nickel species (namely, Ni^{2+}) whose solubility constants were fitted as a function of temperature. The thermodynamic quantities obtained at infinite dilution are: $\log_{10} K^\circ_{s0}$ (25°C) = (11.67 ± 0.20), ΔG°_{s0} (25°C) = −(66.6 ± 1.1) kJ mol^{-1}, ΔH°_{s0} (mean value 5–200°C) = −(82.1 ± 0.8) kJ mol^{-1}, $\Delta_{diss} S^\circ_{s0}$ = (mean value 5–200°C) = −(52 ± 5) J K^{-1} mol^{-1}, ΔC°_p (mean value 5–200°C) = 0 J K^{-1} mol^{-1}, where the uncertainties quoted are 2σ. These results are internally consistent, but differ from most of those reported in the literature. A significantly lower temperature for the thermodynamic stability of β-Ni(OH)$_2$(cr) *versus* NiO(cr), *namely*, 77°C, is proposed based on the current measurements. Additional batch experiments at 50°C and 80°C within aqueous NaClO$_4$ media established and quantified a particle-size dependence of the solubility constant of β-Ni(OH)$_2$(cr) that extended to larger particle sizes than normally observed for metal oxide/hydroxides.

Keywords: Nickel hydroxide; Ni(II); Solubility; Thermodynamics; Aqueous solutions; Temperature; pH; Crystallinity

1. Introduction

Pressurized water reactors (PWRs) of western design constitute approximately 60% of currently operating light-water reactors in the United States, 40% in Japan, nearly 85% in France, and a significant fraction of the nuclear base throughout the rest of Europe and Asia. Water chemistry of the reactor coolant system (RCS) plays a major role in maintaining the safety and reliability of PWRs. The principal objectives of most operational guidelines are to maintain the integrity of the fuel cladding and the primary circuit materials, and to maintain effective radiation management, particularly

*Corresponding author. Email: Solution_Chemistry@comcast.net

Journal of Coordination Chemistry
ISSN 0095-8972 print/ISSN 1029-0389 online
DOI: 10.1080/00958972.2010.492215

during shutdown and startup. As nickel alloys are such important constituents of the construction materials of nuclear plant water circuits, accurate knowledge of nickel thermodynamics is required in estimations of the stability and solubility of these mixed metal phases. Therefore, given improvements made in both experimental equipment and in the sensitivity of analytical techniques required for the measurement of low levels of dissolved nickel, a reinvestigation of the $Ni(OH)_2(s) + H_2O(l)$ system was deemed to be essential.

Kritzer *et al.* [1] discussed the factors controlling corrosion in high-temperature aqueous solutions, including supercritical conditions, in industrial processes, such as salt-separation technologies, extractions, coal cracking, ceramic processing, analytical applications, biomass conversion, and supercritical water oxidation of organic wastes. They listed 12 independent high-temperature solubility studies of NiO/$Ni(OH)_2$(s) and expressed the need for accurate experimental data on the solubility of these and other pure phases related to these corrosion issues. However, in reference to these data for NiO(s) solubility, these authors erroneously state "... this dissolves by forming aquo-complexes (Ni^{2+}_{aq}) in acidic solutions or hydroxy complexes ($[Ni(OH)_6]^{4-}_{aq}$) in alkaline solutions." As the latter species does not exist except in very strong caustic solutions, it is apparent that application of the correct solution chemistry model is also essential in order to interpret experimental results in a thermodynamically rigorous and useful manner.

Macdonald and Cragnolino [2] pointed out that the $Ni(OH)_3^-$ anion increases in stability with increasing temperature, whereas the stability field of Ni^{2+} decreases. This behavior is typical of many metal oxide solubility profiles [3]. However, it should be mentioned that the results of this early study [2] are quite inconsistent with those of subsequent studies including the current one.

It is commonly known that a solid-phase change occurs in the Ni(II)–H_2O system, whereby β-$Ni(OH)_2$(s) is stable at low temperatures, but undergoes dehydration to form NiO(s) [4, 5] at high temperatures. Ziemniak *et al.* [4] observed a discontinuity in the solubility of nickel oxide *versus* temperature curve which was believed to be consistent with a solid-phase change between *ca* 167–195°C. In a more recent study, Ziemniak and Goyette [6] postulated the existence of three nickel(II) solid phases based on their new solubility measurements: hydrous nickel(II) oxide, rhombohedral and cubic nickel(II) oxides. They revised their previous estimate of the β-$Ni(OH)_2$(cr) to NiO(cr) transition to 160°C, whereas the solid-phase transition from a rhombohedral to the anhydrous cubic structure was estimated to occur at 247°C. XPS spectra were presented as evidence for the occurrence of β-$Ni(OH)_2$(cr) in their experiments, but again only NiO(s) was used as the starting material in all their experiments, which were also performed over continuously changing temperature intervals for each feed solution composition rather than isothermally. These conclusions were not substantiated in the present study. The 1982 NBS compilation of Wagman *et al.* [7] predicted a positive Gibbs energy change for the hydration of NiO(cr) to form β-$Ni(OH)_2$(cr) of 1.6 kJ mol^{-1} at 25°C. Note that Tremaine and LeBlanc [8] were unable to obtain thermodynamic information on the solubility of nickel metal at high temperatures due to oxidation of the metal surface to the oxide and hydroxide phases, despite efforts to remove oxygen from the system. Low-temperature solubility data for nickel(II) hydroxide reported until 1997 suffer from uncertainty as to the nature of the physical state of the solid investigated. Mattigod *et al.* [9] were the first to characterize the initial solid material and final equilibrated solid phases using X-ray diffraction (XRD).

Moreover solid/liquid equilibrium was approached from both oversaturation and undersaturation in their study.

More recently, Gamsjäger *et al.* [5] reported measurements of the solubility of β-$Ni(OH)_2$(cr) from 35°C to 80°C in acidic solutions (i.e., where Ni^{2+} is the dominant nickel species in solution) and confirmed that large discrepancies exist in previously published results.

2. Experimental

2.1. *Hydrogen-electrode concentration cell*

The use of this cell obviates the need to control pH either by addition of excess acid or base, in which case the pH must be determined by a mass-balance calculation that also requires knowledge of the nickel species in solution, or through the use of pH buffering agents that were necessary in the flow-through experiments reported here. In the latter case, there is always concern that the buffering agent will complex Ni^{2+} ions, requiring low concentrations and even then agents, such as ammonia, cannot be employed at temperatures $\leq$200°C because it forms strong complexes at low temperatures. Furthermore, for the flow-through experiments at low to moderate temperatures, the use of excess acid was impossible because the solubility of β-$Ni(OH)_2$(cr) was too high to allow an accurate mass-balance calculation to be made, i.e., virtually all the free acid was consumed. Conversely, the HECC was only applicable at relatively low pH, because reduction of the dissolved nickel by the prevailing hydrogen atmosphere became evident at pH values where hydrolysis became significant.

The general design and function of the HECC as applied to solubility measurements have been described previously, e.g., Palmer *et al.* [10]. A solution of known stoichiometric hydrogen ion molality in the inner Teflon cup served as the pH reference, whereas the same solution in the outer cup, referred to as the test solution, contained a suspension of β-$Ni(OH)_2$(cr) (typically *ca* 1 g of solid in *ca* 65 mL of solution). In the head space of the cell, a 4 : 1 Ar/H_2 gas mixture was used instead of pure hydrogen in order to minimize reduction of the solid phase to metallic nickel. Temperature control was generally better than ±0.1°C. Sodium trifluoromethanesulfonate, F_3CSO_3Na, was the electrolyte of choice to fix the ionic strength at 0.03 mol kg^{-1}, which is about the minimum ionic strength that can be maintained to ensure its dominance over other ions in solution in these experiments. It was prepared by careful addition of a sodium hydroxide solution, $w(NaOH) = 0.5$, into a well-stirred solution of the acid (Alfa Aesar, 98%) in ethanol. The resulting solid was recrystallized twice from hot ethanol.

The initial configuration of the cell in a typical β-$Ni(OH)_2$(cr) solubility experiment involved acidic reference and test solutions (separated by the liquid junction, ‖) as follows:

$$\underset{}{H_2,Pt} \;\big|\; \underbrace{\underset{m_1}{F_3CSO_3H},\; \underset{m_2}{F_3CSO_3Na}}_{\text{reference}} \;\|\; \underbrace{\underset{m_1}{F_3CSO_3H},\; \underset{m_2}{F_3CSO_3Na},\; \beta\text{-}Ni(OH)_2(cr)}_{\text{test}} \;\big|\; \underset{}{Pt,H_2}$$

In general, the ratio $m_1 : m_2$ was <0.1 in order to minimize both the liquid-junction contribution to the measured potential and activity coefficient differences between the two solutions. Aliquots of the test solution were withdrawn through a platinum dip tube gold-welded to a porous platinum frit to prohibit particles from entering the tube, because their presence could have served as seeds promoting precipitation during the sampling process. Samples were withdrawn *via* a titanium valve and a 0.2 μm fluoropolymer filter into pre-weighed polypropylene syringes containing a known mass of high purity 0.2% HNO_3 (JT Baker Ultrex Reagent) for subsequent chemical analysis of the nickel content.

The hydrogen ion molality in the test compartment, m_{H^+}, was determined relative to the known molality in the reference compartment, $m_{1\text{ref}}$, from the Nernst equation:

$$pH_m \equiv -\log_{10} m_{H^+} = \log_{10} m_{1\,\text{ref}} + F(E + E_{LJ})/(RT \ln 10), \quad (1)$$

where E is the measured cell potential, E_{LJ} is the estimated liquid-junction potential calculated from the complete Henderson equation as presented by Baes and Mesmer [11], and F, R, and T represent the Faraday constant, the universal gas constant, and the temperature in kelvin, respectively. The largest E_{LJ} values were recorded for the 0.03 mol kg^{-1} ionic strength titrations (i.e., $|E_{LJ}| = 4.8$ mV when the test solution was near neutral pH_m, leading to an uncertainty in pH_m of *ca* 0.01 [11]).

Note that in experiments conducted at ≥150°C, some nickel metal was discovered (verified by XRD analysis) in the test cup after the experiment was terminated.

2.2. *High-temperature flow-through cell*

This apparatus was first described by Bénézeth *et al*. [12] and was used here for measurements from 100°C to 200°C. It is important to note that downstream from the outlet closure piece of the cylindrical pressure vessel, a short section of larger diameter platinum/rhodium tubing was welded into the sampling line and served as a mixing chamber, which allowed a 0.6% nitric acid solution to be pumped into the saturated nickel outlet stream at the experimental temperature and pressure, thereby ensuring that nickel (hydroxide/oxide) did not deposit from solution as it cooled prior to collection of the sample. The temperature and pressure stabilities of this apparatus were <±0.2°C and <0.1 MPa, respectively.

Dilute boric acid and sodium monohydrogen-dihydrogen phosphate pH buffers were used and their concentrations were varied to test for complexation effects with Ni^{2+}.

2.3. *Low-temperature flow-through cell*

This apparatus was utilized for two solubility measurements at 25°C and incorporated commercially available components, principally three polyetheretherketone (PEEK) chromatography columns (25 cm long × 7.5 mm in diameter) connected in series *via* PEEK tubing. The columns were submerged in a water bath at (25.0 ± 0.1)°C. The outlet stream was collected into a weighed polypropylene syringe into which, in most cases, a weighed amount of 0.2% ultra pure nitric acid had been added. The syringe and PEEK tubing leading to it were also immersed in the bath as a precaution against deposition before the sample reached the acidified solution in the syringe. The flow rate

was varied in the initial series of experiments, but, thereafter it was maintained at $0.02\,mL\,min^{-1}$. The approximate residence time for the feed solution in the β-$Ni(OH)_2$(cr) bed was 10 h. Many days of flushing the columns, often at enhanced flow rates, were necessary to establish equilibrium. Note that due to the strong complexation of nickel(II) ions by ammonia at 25°C, boric acid was used as a pH buffer in these experiments. Additional experiments were attempted from 40°C to 75°C using a dilute NaOH solution to determine K_{s2} but these failed to produce useful results.

2.4. *Preparation and characterization of the $Ni(OH)_2$ solid phase*

Nickel hydroxide was obtained in very pure form commercially (Aldrich Chemical Co.), but only as ultra-fine, irregular-shaped particulates that exhibited characteristic broad XRD peaks. All attempts to recrystallize this commercial material from various aqueous solutions failed. However, in the early stages of this study, a method for direct preparation of well-defined crystalline β-$Ni(OH)_2$ became available [5]. A slightly modified method was developed in which 800 g of a solution $w(NaOH) = 0.5$ (Mallinckrodt AR grade) was contained in a 1 L capacity Teflon Savillex® vessel containing a "spin-fin" Teflon-coated magnetic stirrer. The vessel was placed into a bath containing ethylene glycol, mounted on a stirrer – hot plate which controlled the temperature to (140 ± 2)°C. A glass air condenser penetrated the Teflon lid of the vessel, while through another port in the lid a 0.159 cm OD PEEK® tube was connected *via* a Teflon valve to a Teflon beaker that held approximately 55 g of $Ni(ClO_4)_2 \cdot 6H_2O$ (Aldrich Chemical Co., 99.999%) or 40 g of $NiCl_2 \cdot 6H_2O$ (Alfa Aesar, 99.95%) dissolved in 25 g of water. The beaker was elevated to *ca* 10 cm above the top of the vessel such that when the Teflon valve was opened the nickel solution siphoned dropwise into the hot, stirring NaOH solution. After the nickel solution had been added, the mixture was maintained at 140°C overnight, whereupon the heater was turned off to allow the system to cool slowly to room temperature. The excess NaOH was decanted off and distilled water added. This washing – decanting cycle was repeated several times before dilute nitric acid was added until the solution remained mildly acidic, whereupon it was allowed to stir overnight on a warm hot plate. The mixture was then filtered under vacuum through a large sintered-glass Büchner funnel. The light-green precipitate was then repeatedly washed with deionized water until the filtrate was virtually pH neutral. The $Ni(OH)_2$ crystals were finally washed with ethanol followed by acetone and then dried in a vacuum oven at 60°C. The yield was *ca* 20 g. Multiple batches were prepared during the course of this study although, unfortunately, no detailed record was kept of which batch was used in each run with the exception of the last three in which samples supplied by Prof. Gamsjäger were used. The Raman spectrum of the solid prepared in this manner exhibited an intense, sharp band at $3076.2\,cm^{-1}$ with other minor bands and shoulders.

An XRD pattern and SEM image of these crystals are shown in figures 1 and 2. A BET (nitrogen) surface-area analysis yielded $(2.86 \pm 0.07)\,m^2\,g^{-1}$. The grains were approximately 3 μm across, which is far less than reported by Gamsjäger *et al.* [5], and Wallner and Gatterer [13].

Note that the XRD pattern of solid β-$Ni(OH)_2$(cr) recovered from the HECC after completion of experiment 9 was identical to that shown in figure 1. This experiment was

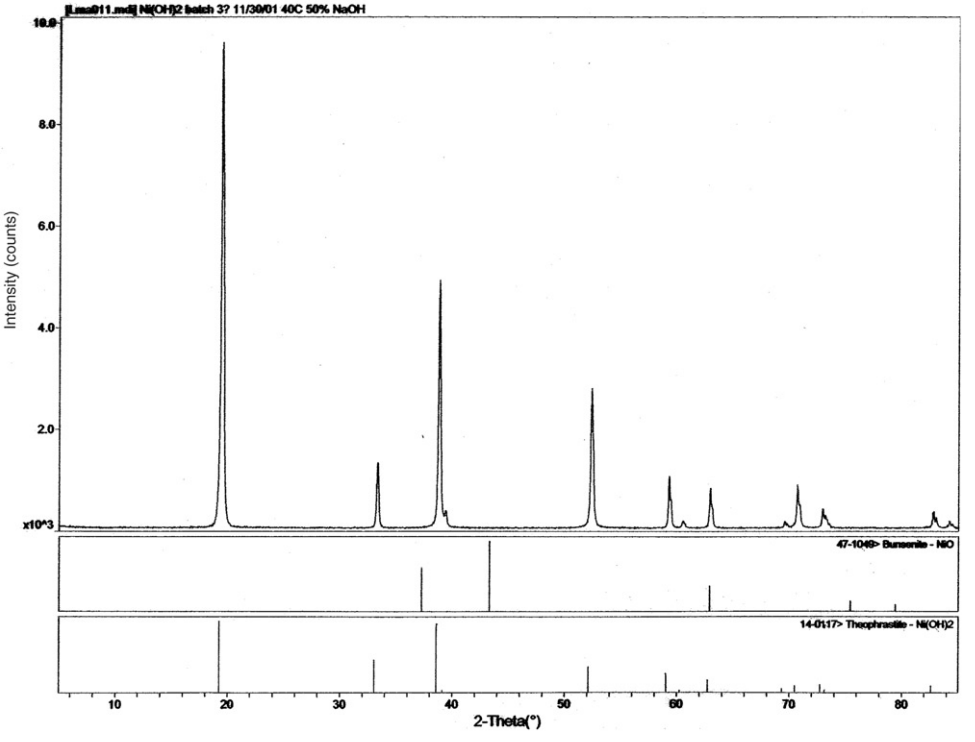

Figure 1. XRD pattern of β-Ni(OH)$_2$(cr) prepared by the modified method of Gamsjäger *et al.* [5] showing sharp, narrow peaks that are characteristic of well-crystallized nickel hydroxide (trigonal, space group: $P\bar{3}m1$, with cell dimensions $a = 3.126$ Å, $c = 4.605$ Å, $Z = 1$ – JCPDS-ICDD card no. 124-117).

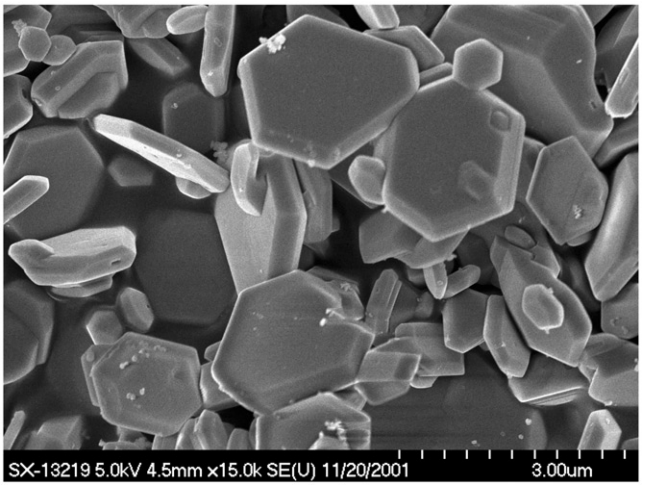

Figure 2. SEM images of hexagonal plate-like crystals of β-Ni(OH)$_2$(cr) prepared by the modified method of Gamsjäger *et al.* [5].

begun at 100°C and completed at 0.5°C, over a period of 8 days, including the initial 48 h at 100°C required to obtain a stable potential reading.

An XRD pattern was also taken of the washed solid recovered from the HECC after experimental series 10, which was finally maintained at 199.7°C for 26 h, and clearly indicated the presence of metallic nickel with perhaps the suggestion that a minor amount of NiO had also formed, but the major NiO diffraction peak was almost indistinguishable from the baseline noise. The XRD pattern of a β-$Ni(OH)_2$ solid sample recovered from the outlet of the high-temperature flow cell after completing the series 150-ht at 150°C showed no evidence of any other phase having been formed after 28 days at this temperature and previously after 46 days at 100°C. Apparently, the bulk dehydration of the β-$Ni(OH)_2$ crystals is relatively slow even at 200°C, consistent with the continued existence of this meta-stable phase (two samples were taken at this temperature after 20 and 26 h with no discernable differences in the concentration of nickel in solution or pH_m).

2.5. *TGA analysis of the nickel hydroxide – nickel oxide transition*

TGA analyses of the dehydration of β-$Ni(OH)_2$(cr) to ($NiO(cr) + H_2O(g)$) were performed over a range of heating rates in order to constrain and, if possible estimate, the temperature at which the reaction proceeded to completion. Initial dehydration temperatures were obtained by taking the first derivative of the TGA data and finding the point at which the curve first dropped below zero, outside the range of scatter in the data. These temperatures were then plotted as a function of the heating rate of the TGA experiment. Extrapolation back to "zero" rate was difficult, because the transition temperature changed more rapidly on approach to "zero" heating rate. However, these results at least constrain the upper temperature of the dehydration reaction to less than 179°C. Based on their solubility constants, Ziemniak *et al.* [4] estimated 195°C as the transition temperature, whereas Mukaibo *et al.* [14] had earlier estimated 167°C. The TGA data presented here with an upper limit of 179°C support the conclusions of the latter study. Swaddle and Wong [15] measured the dehydration kinetics in aqueous solution and concluded that the reaction is sluggish. Ziemniak *et al.* [4] neither prepared nor characterized solid $Ni(OH)_2$(cr), which was assumed to have formed near 167°C during a sequence of NiO(cr) flow-cell solubility measurements carried out at descending temperature intervals. Similarly, Tremaine and LeBlanc [8] measured the solubility of NiO(cr) from 150°C to 300°C and reported a solubility constant, K_{s0}, of $Ni(OH)_2$ at 100°C, but they also did not prepare or characterize this solid and appear to have determined this value from existing literature data.

Based on a private communication from Dr Malcolm Rand, UK, figure 3 was derived from thermodynamic data for NiO(cr) [16] and older, less precise data for β-$Ni(OH)_2$(cr) [17]. This plot of the Gibbs energy for the dehydration of β-$Ni(OH)_2$(cr) to yield NiO(cr) and $H_2O(g)$ *versus* temperature in kelvin gives a temperature for a zero-energy change of 350 K (77°C), which is considerably below the temperatures cited above.

2.6. *Sample handling and analytical methods*

Samples were collected directly into either polyethylene bottles, which had been presoaked in 0.2% nitric acid for at least 24 h and rinsed with Nanopure water, or into

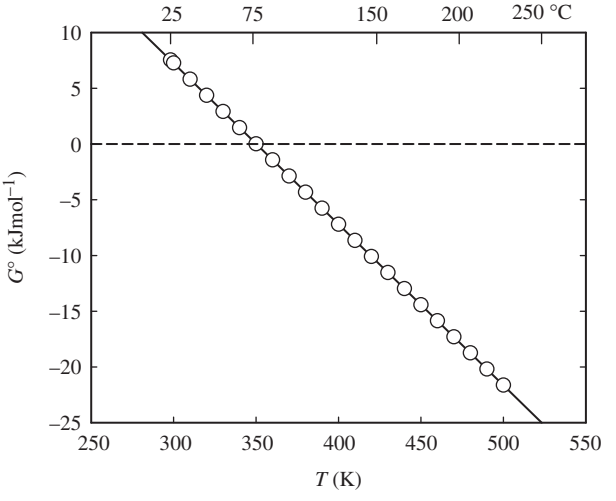

Figure 3. Plot of the Gibbs energy change for the transformation reaction, β-Ni(OH)$_2$(cr) → NiO(cr) + H$_2$O(g), as a function of temperature in kelvin.

polypropylene disposable syringes containing 0.2% nitric acid prepared by dilution of 70% JT Baker Ultrex Reagent nitric acid. Stock solutions of NaOH, F_3CSO_3H, $B(OH)_3$, and NaH_2PO_4 were prepared from ultra-pure reagents: 50% (by weight) NaOH solution (Mallinckrodt AR grade); concentrated F_3CSO_3H (Alfa Aesar) purified by vacuum distillation; solid $B(OH)_3$ (US Borax, 99.9%); and NaH_2PO_4 (Aldrich Chemical Co., 99.999%). These solutions were prepared with de-aerated, distilled, deionized water and kept under either a helium or argon overpressure.

Nickel analyses were performed by the following techniques depending on the nickel concentration in the sample: atomic absorption utilizing a graphite furnace (Perkin Elmer 4110ZL) or a flame (Perkin Elmer 3110) spectrophotometer; an ICP (Thermo Jarrell Ash IRIS), or ICP–MS (Finnigan MAT ELEMENT) two double-focusing sector field (SF)–ICP–MS.

3. Results

3.1. *Thermodynamic background*

The equilibria considered initially in treatment of the dissolution data for nickel hydroxide in aqueous solutions were as follows:

$$\beta\text{-Ni(OH)}_2\text{(cr)} + 2\,\text{H}^+ \rightleftarrows \text{Ni}^{2+} + 2\,\text{H}_2\text{O(l)} \tag{2}$$

$$\beta\text{-Ni(OH)}_2\text{(cr)} + \text{H}^+ \rightleftarrows \text{Ni(OH)}^+ + \text{H}_2\text{O(l)} \tag{3}$$

$$\beta\text{-Ni(OH)}_2\text{(cr)} \rightleftarrows \text{Ni(OH)}_2^0 \tag{4}$$

$$\beta\text{-Ni(OH)}_2\text{(cr)} + 1.5\,\text{H}^+ \rightleftarrows 0.5\,\text{Ni}_2\text{(OH)}^{3+} + 1.5\,\text{H}_2\text{O(l)} \tag{5}$$

$$\beta\text{-Ni(OH)}_2\text{(cr)} + \text{H}^+ \rightleftarrows 0.25\,\text{Ni}_4\text{(OH)}_4^{4+} + \text{H}_2\text{O(l)} \tag{6}$$

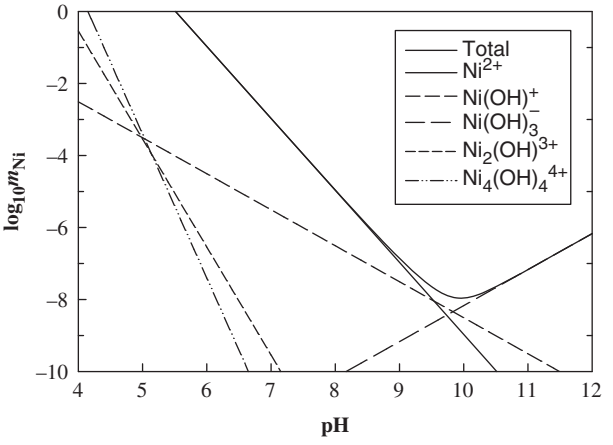

Figure 4. Speciation plot for Ni(II) species in solution based on the NEA [18] recommended values at 25°C where β-$Ni(OH)_2$(cr) is the solubility determining solid phase.

In their thorough review of nickel chemistry, Gamsjäger *et al.* [18] recommended Gibbs energy values at 25°C for only Ni^{2+}, $Ni(OH)^{+}$, $Ni(OH)_3^{-}$, $Ni_2(OH)^{3+}$, and $Ni_4(OH)_4^{4+}$ obtained from potentiometric, solubility and kinetic measurements. Based on these NEA approved values, together with those of β-$Ni(OH)_2$(cr) and H_2O(l), the solubility diagram shown in figure 4 was constructed at 25°C, clearly indicating that the dimer and tetramer are unstable at nickel concentrations controlled by the presence of the nickel hydroxide solid phase. Note that as with most multinuclear metal hydroxo complexes, the stabilities of the dimer and tetramer decrease substantially with increasing temperature and were therefore not considered further in the treatment of the solubility data. The $Ni(OH)^{+}$ species is also shown to be a minor species in this plot with a field of dominance from pH 9.6 to 9.8 making it very difficult to derive the solubility constant for this species with any certainty.

The solubility constants with the appropriate activity coefficients and water activities are derived from:

$$K^{o}_{s0} = m_{Ni^{2+}}\gamma_{Ni^{2+}}a_w^2/m_{H^+}^2\gamma_{H^+}^2 = Q_{s0}\gamma_{Ni^{2+}}a_w^2/\gamma_{H^+}^2, \quad (7)$$

where $\gamma_{Ni^{2+}}$ is the activity coefficient of Ni^{2+}, γ_{H^+} is the activity coefficient of hydrogen ion and a_w is the activity of water.

In view of the low ionic strengths employed, the stoichiometric activity coefficient of Ni^{2+} was derived from Meissner's equation [19] with the implicit assumption that for an ion of charge, z: $\gamma_{|z|} = \gamma_{\pm(NaCl)}^{z^2}$, where $\gamma_{\pm(NaCl)}$ is the molal activity coefficient of NaCl. The advantage of this approach is that accurate $\gamma_{\pm(NaCl)}$ values are available over the temperature range accessed in this investigation [20]. The corresponding activities of water were also taken from Archer [20].

3.2. *HECC experiments*

The temperature was cycled in different directions from different starting values to gauge whether true equilibrium conditions had been achieved. The cycling

of temperature is equivalent to approaching the equilibrium solubility from undersaturation and oversaturation. Most of the HECC experiments were begun at 100°C rather than at 25°C to accelerate the initial approach to equilibrium, and the same results were obtained within the combined experimental error, again indicating that thermodynamic equilibrium was established throughout. The experimental results presented in table 1 were confined to the pH region where Ni^{2+} is the dominant nickel species in solution. This condition was tested by conducting the titrations at two different starting acidities with a common molal ionic strength of 0.03 mol kg^{-1} (runs 1–7 and 10–13 in 0.001–0.0011 mol kg^{-1} H^+, respectively, and runs 8 and 9 in 0.003 mol kg^{-1} H^+) with identical results obtained in all cases. Furthermore, knowledge of the hydrolysis constants of Ni^{2+} confirmed that hydrolysis could be ignored in the pH_m ranges covered in these experiments [18]. The time intervals from the start of each experiment to the first sampling event and then the following time intervals between samplings are tabulated to demonstrate that equilibration was indeed obtained rapidly in this cell, even at temperatures approaching 0°C.

It is apparent from scrutiny of all the data in table 1 that the self-buffering effect due to the dissolution of β-Ni(OH)$_2$(cr) resulted in rather constant nickel concentrations in most of these experiments. The pH_m values, on the other hand, varied markedly and provided a sensitive indicator of the attainment of equilibrium. Therefore, solution samples were only taken when the pH_m reading reached a constant value. The surprising speed with which equilibrium was attained with the HECC is attributed to the efficient stirring effect that kept the solid particles suspended exposing all surfaces to the solution. Note that the use of a "spin-fin" Teflon-coated magnet in a Teflon cup prevented any physical degradation of the solid particles as reflected by the constant BET surface-area analyses of the particles measured before and after such experiments.

3.3. *High-temperature flow-through cell experiments*

In these experiments, summarized in table 2, both boric acid–sodium borate and sodium dihydrogen phosphate–disodium monohydrogen phosphate mixtures were used to buffer the pH_m.

For the phosphate buffer, the first- and second-base hydrolysis constants of phosphoric acid were taken from Mesmer and Baes [21]:

$$H_3PO_4^0 + OH^- \rightleftarrows H_2PO_4^- + H_2O(l)$$

$$\log_{10} Q_{b1} = -253.198 + 1.76558 \times 10^4/T + 39.4277 \ln(T) - 3.25405 \times 10^{-2} T - 8.10134 \times 10^5 T^2 - 0.152147 I_m + 0.00105195 I_m T + 0.140119 I_m^{1.5} - 0.00131413 T I_m^{1.5}, \quad (8)$$

$$H_2PO_4^- + OH^- \rightleftarrows HPO_4^{2-} + H_2O(l)$$

$$\log_{10} Q_{b2} = -246.045 + 1.71569 \times 10^4/T + 37.7345 \ln(T) - 3.22082 \times 10^{-2} T - 8.97579 \times 10^5 T^2 + 2AI_m^{0.5}/[1 + (-0.110812 + 0.0113329T)A' I_m^{0.5}] - 0.525884 I_m + 0.0019989 I_m T + 0.453717 I_m^{0.5} - 0.00140089 T I_m^{0.5}, \quad (9)$$

Table 1. Summary of the treatment of results for the solubility of β-Ni(OH)$_2$ from the HECC experiments.[a]

Run no.	Δ(time) (h)	t (°C)	p (MPa)	a_w	I_m	pH_m	$\gamma_{\pm(NaCl)}$	$\log_{10} m_{Ni}$	$\log_{10} K^{o}_{s0}$
1–1	139	50.2	2.3	0.9989	0.0309	6.341	0.842	−3.150	9.38
1–2	6	50.2	2.6	0.9989	0.0309	6.383	0.842	−3.154	9.46
1–3	21	50.2	2.6	0.9989	0.0309	6.356	0.842	−3.150	9.41
1–4	24	50.2	2.6	0.9989	0.0309	6.356	0.842	−3.153	9.41
1–5	24	50.0	2.6	0.9989	0.0309	6.358	0.842	−3.147	9.42
1–6	22	50.0	2.7	0.9989	0.0309	6.359	0.843	−3.147	9.42
1–7	22	50.2	3.5	0.9989	0.0309	6.357	0.843	−3.148	9.42
1–8	9	100.0	4.4	0.9990	0.0308	5.360	0.826	−3.186	7.37
1–9	20	99.9	4.8	0.9990	0.0308	5.354	0.826	−3.189	7.35
1–10	15	149.8	6.4	0.9990	0.0307	5.000	0.803	−3.222	6.59
1–11	5	149.8	7.2	0.9990	0.0307	5.047	0.803	−3.225	6.68
2–1	28	75.0	1.8	0.9989	0.0309	6.504	0.835	−3.160	9.69
2–2	18	75.0	2.0	0.9989	0.0309	6.500	0.835	−3.160	9.68
2–3	23	74.9	2.6	0.9989	0.0309	6.501	0.835	−3.158	9.69
2–4	26	99.9	3.4	0.9990	0.0308	6.079	0.826	−3.176	8.82
2–5	22	100.0	4.1	0.9990	0.0308	6.065	0.826	−3.171	8.79
2–6	24	99.9	4.7	0.9990	0.0309	6.080	0.826	−3.165	8.83
2–7	21	150.0	6.0	0.9990	0.0308	5.242	0.803	−3.191	7.10
2–8	29	150.0	6.5	0.9990	0.0308	5.270	0.803	−3.197	7.15
2–9	10	150.0	6.5	0.9990	0.0308	5.270	0.803	−3.196	7.15
3–1	25	74.9	2.1	0.9989	0.0309	6.449	0.835	−3.154	9.59
3–2	16	74.9	2.4	0.9989	0.0309	6.434	0.835	−3.151	9.56
3–3	7	74.9	3.0	0.9989	0.0309	6.435	0.835	−3.155	9.56
3–4	17	50.1	2.7	0.9989	0.0309	6.888	0.842	−3.145	10.48
3–5	31	50.2	3.0	0.9989	0.0309	6.937	0.842	−3.142	10.58
3–6	23	50.1	3.0	0.9989	0.0309	6.938	0.842	−3.140	10.59
3–7	20	50.1	3.2	0.9989	0.0309	6.947	0.842	−3.140	10.60
5–1	41	99.9	3.5	0.9990	0.0307	6.115	0.826	−3.210	8.85
5–2	7	99.9	4.2	0.9990	0.0307	6.109	0.826	−3.203	8.85
5–3	15	50.2	3.7	0.9989	0.0308	6.981	0.843	−3.164	10.65
5–4	9	50.1	3.8	0.9989	0.0309	6.974	0.843	−3.141	10.66
5–5	15	99.9	5.6	0.9990	0.0307	6.127	0.826	−3.212	8.88
6–1	145	25.0	3.3	0.9989	0.0308	7.494	0.849	−3.177	11.67
6–2	23	25.0	3.4	0.9989	0.0308	7.485	0.849	−3.175	11.65
6–3	25	49.7	3.8	0.9989	0.0308	6.861	0.843	−3.174	10.40
6–4	21	49.6	3.8	0.9989	0.0308	6.844	0.843	−3.175	10.36
6–5	22	24.9	3.9	0.9989	0.0308	7.417	0.849	−3.166	11.52
7–1	47	50.3	2.9	0.9989	0.0307	7.052	0.843	−3.213	10.74
7–2	7	50.2	3.0	0.9989	0.0307	7.044	0.843	−3.215	10.72
7–3	21	24.8	2.9	0.9989	0.0307	7.549	0.849	−3.212	11.74
7–4	25	24.7	3.3	0.9989	0.0307	7.562	0.849	−3.212	11.77
7–5	22	24.8	3.4	0.9989	0.0307	7.549	0.849	−3.209	11.75
7–6	21	24.6	3.4	0.9989	0.0307	7.568	0.849	−3.210	11.78
7–7	9	0.6	3.5	0.9989	0.0307	8.055	0.853	−3.209	12.76
7–8	24	24.9	5.0	0.9989	0.0307	7.520	0.849	−3.214	11.68
7–9	15	24.9	5.2	0.9989	0.0307	7.533	0.849	−3.211	11.71
7–10	9	49.9	5.9	0.9989	0.0307	6.897	0.843	−3.209	10.44
7–11	15	49.9	6.7	0.9989	0.0307	6.858	0.843	−3.214	10.35
8–1	19	100.0	3.1	0.9990	0.0306	6.040	0.826	−3.254	8.66
8–2	5	100.0	3.6	0.9990	0.0306	6.051	0.826	−3.251	8.68
8–3	24	99.8	3.7	0.9990	0.0306	6.043	0.826	−3.253	8.67
8–4	42	75.0	4.1	0.9989	0.0306	6.494	0.835	−3.247	9.58
8–5	8	75.0	4.4	0.9989	0.0306	6.483	0.835	−3.241	9.57
8–6	15	49.9	4.0	0.9989	0.0306	6.932	0.843	−3.238	10.48
8–7	27	50.0	4.2	0.9989	0.0306	6.966	0.843	−3.236	10.55
8–8	6	24.8	4.6	0.9989	0.0306	7.491	0.849	−3.232	11.61
8–9	15	24.8	4.7	0.9989	0.0306	7.509	0.849	−3.231	11.64

(*Continued*)

Table 1. Continued.

Run no.	Δ(time) (h)	t (°C)	p (MPa)	a_w	I_m	pH_m	$\gamma_{\pm(NaCl)}$	$\log_{10} m_{Ni}$	$\log_{10} K^o_{s0}$
8–10	10	24.7	4.9	0.9989	0.0306	7.516	0.849	−3.227	11.66
8–11	20	0.3	4.1	0.9989	0.0307	8.068	0.853	−3.221	11.64
9–1	41	99.9	4.2	0.9990	0.0319	5.867	0.824	−2.754	8.81
9–2	9	99.9	4.8	0.9990	0.0319	5.869	0.824	−2.762	8.81
9–3	15	75.0	5.0	0.9989	0.0319	6.289	0.833	−2.751	9.67
9–4	32	75.0	5.4	0.9989	0.0320	6.295	0.833	−2.740	9.69
9–5	15	50.2	5.0	0.9989	0.0319	6.747	0.841	−2.751	10.59
9–6	9	46.5	5.7	0.9989	0.0320	6.825	0.842	−2.746	10.75
9–7	27	24.2	5.2	0.9989	0.0320	7.339	0.847	−2.744	11.79
9–8	5	24.2	5.4	0.9989	0.0320	7.339	0.847	−2.742	11.79
9–9	18	6.5	4.7	0.9989	0.0321	7.758	0.850	−2.737	12.65
9–10	26	5.6	5.0	0.9989	0.0319	7.783	0.850	−2.757	12.67
9–11	27	0.5	5.8	0.9989	0.0321	7.957	0.850	−2.732	13.04
10–1	24	99.9	3.3	0.9990	0.0307	6.026	0.826	−3.182	8.70
10–2	20	99.8	3.8	0.9990	0.0307	6.050	0.826	−3.179	8.75
10–3	26	149.9	4.9	0.9990	0.0307	5.367	0.803	−3.179	7.36
10–4	19	149.8	5.4	0.9990	0.0308	5.368	0.803	−3.139	7.41
10–5	23	199.7	8.9	0.9990	0.0307	4.826	0.772	−3.182	6.24
10–6	6	199.7	10.3	0.9990	0.0307	4.830	0.773	−3.198	6.24
11–1[b1]	70	99.9	3.0	0.9990	0.0302	5.317	0.827	−3.168	8.75
11–2	31	99.9	3.0	0.9990	0.0302	5.358	0.827	−3.167	8.84
11–3	15	100.0	3.2	0.9990	0.0302	5.376	0.846	−3.159	8.91
11–4	24	50.6	3.2	0.9990	0.0302	6.260	0.844	−3.102	10.86
11–5	8	50.6	3.3	0.9990	0.0302	6.230	0.844	−3.131	10.77
11–6	16	50.4	3.5	0.9990	0.0302	6.209	0.844	−3.131	10.73
11–7	53	25.4	3.8	0.9990	0.0302	6.841	0.850	−3.073	12.14
11–8	28	25.4	4.0	0.9990	0.0302	6.833	0.850	−3.076	12.12
11–9	25	6.3	4.2	0.9990	0.0302	7.046	0.854	−3.106	12.54
11–10	7	5.1	4.4	0.9990	0.0302	7.113	0.853	−3.048	12.74
11–11	14	5.1	4.4	0.9990	0.0302	7.116	0.853	−2.998	12.80
11–12	24	25.6	5.9	0.9990	0.0302	6.771	0.850	−3.039	12.02
12–1[b2]	46	100.0	3.7	0.9990	0.0308	6.155	0.825	−3.247	8.895
12–2	7	100.0	3.7	0.9990	0.0308	6.160	0.825	−3.244	8.908
12–3	17	75.0	3.7	0.9989	0.0309	6.568	0.834	−3.205	9.773
12–4	4	75.1	3.6	0.9989	0.0309	6.565	0.834	−3.198	9.774
12–5	20	50.0	3.6	0.9989	0.0309	6.997	0.842	−3.219	10.625
12–6	7	50.0	3.6	0.9989	0.0310	6.996	0.842	−3.167	10.675
12–7	17	49.9	3.6	0.9989	0.0310	7.003	0.842	−3.163	10.693
12–8	23	25.0	3.5	0.9989	0.0310	7.365	0.848	−3.166	11.419
12–9	6	25.0	3.5	0.9989	0.0311	7.400	0.848	−3.144	11.512
12–10	18	25.0	3.4	0.9989	0.0310	7.391	0.848	−3.164	11.474
13–1[b2]	49	100.0	3.5	0.9990	0.0307	6.123	0.825	−3.284	8.794
13–2	25	100.1	3.4	0.9990	0.0307	6.128	0.825	−3.274	8.815
13–3	44	95.0	3.3	0.9989	0.0308	6.554	0.835	−3.233	9.717
13–4	23	75.0	3.3	0.9989	0.0308	6.549	0.835	−3.237	9.703
13–5	24	50.3	3.2	0.9989	0.0309	6.977	0.842	−3.196	10.608
13–6	26	50.3	3.2	0.9989	0.0309	6.984	0.842	−3.201	10.617
13–7	24	50.4	3.2	0.9989	0.0309	6.986	0.842	−3.198	10.624
13–8	27	24.8	3.1	0.9989	0.0310	7.419	0.848	−3.178	11.516
13–9	19	24.7	3.1	0.9989	0.0310	7.435	0.848	−3.173	11.553
13–10	24	24.7	3.1	0.9989	0.0310	7.430	0.848	−3.172	11.544
13–11	24	24.7	3.0	0.9989	0.0312	7.441	0.848	−3.131	11.607
13–12	100	5.3	3.0	0.9989	0.0311	7.771	0.851	−3.150	12.251
13–13	18	5.5	3.1	0.9989	0.0311	7.744	0.851	−3.150	12.197

[a]The experimental uncertainty (2σ) in $\log_{10} K^o_{s0}$ was determined to be 0.10 with the most significant contribution coming from the pH_m measurement.
[b]The β-Ni(OH)$_2$(cr) used in these experiments was supplied by Prof. Gamsjäger ([b1]batch 1, [b2]batch 2).

Table 2. Summary of results for the solubility of β-$Ni(OH)_2$(cr) from the high-temperature flow-cell experiments with flow rates of 0.1 and 0.3 mL m^{-1} for the $B(OH)_3$ and PO_4 buffer feed solutions, respectively (water activities are taken as 1.0000; No sam. refers to the number of samples analyzed; Δtime corresponds to the total duration of each experiment).[a,b]

t (°C)	No. sam.	Δtime (h)	Buffer	$m_{buffer} \times 10^{-3}$	$m_{NaOH} \times 10^{-4}$	$I_m \times 10^{-3}$	pH_m	$\gamma_{\pm(NaCl)}$	$\log_{10} m_{Ni}$	$\log_{10} K^o_{s0}$
100.0	13	218	$B(OH)_3$	2.028	0	0.13	7.019	0.989	-4.46 ± 0.08	9.57
100.0	12	74	$B(OH)_3$	0.274	0	0.06	7.899	0.991	-4.68 ± 0.06	11.11
100.0	10	148	PO_4	0.105	5.12	2.11	6.919	0.942	-5.52 ± 0.06	8.27
100.0	14	211	PO_4	0.239	1.26	0.49	7.016	0.971	-5.62 ± 0.02	8.39
150.0	14	216	PO_4	1.046	5.02	2.00	7.155	0.936	-6.37 ± 0.03	7.88
150.0	11	120	PO_4	0.280	1.40	0.56	7.211	0.965	-6.48 ± 0.03	7.92
150.0	16	311	PO_4	2.022	2.00	2.44	6.456	0.930	-5.36 ± 0.18	7.48

[a]The $\log_{10} m_{Ni}$ values represent the average from multiple samples collected at each condition and the associated uncertainties are simply the averages of these analyses.
[b]The experimental uncertainty (2σ) in $\log_{10} K^o_{s0}$ was determined to be 0.17 with the most significant contribution coming from the pH_m measurement.

where

$$A' = 0.4125A^{1/3}, \tag{10}$$

$$\begin{aligned} A' = &-2.97627 + 4.80688 \times 10^{-2}T - 2.69280 \times 10^{-4}T^2 \\ &+ 7.49524 \times 10^{-7}T^3 - 1.02352 \times 10^{-9}T^4 \\ &+ 5.58004 \times 10^{-13}T^5. \end{aligned} \tag{11}$$

For the series in which boric acid was used to buffer the pH_m of the solution, the following expression was used for the acid dissociation constant [22]:

$$\begin{aligned} \log_{10} Q_a = &\ 3645.18/T + 11.6402 \log_{10} T + (16.4914 - 0.023917T) \log_{10} \rho_w \\ &- 36.2605 - 0.11902I_m - 36.3613I_m FI/T - 0.72132I_m^2 \log_{10} \rho_w, \end{aligned} \tag{12}$$

where $FI = (1.0 - (1.0 + 2.0I_m^{0.5})e^{(-2.0I_m^{0.5})})/(2.0I_m)$ and ρ_w is the density of water, g cm^{-3}.

The appropriate dissociation constant of water was calculated at temperature, T, from Marshall and Franck [23] and the Meissner-based activity coefficients were calculated to determine Q_w at ionic strength I_m. Taking into account the dissolution of β-$Ni(OH)_2$(cr), the pH_m values were then determined within an iterative loop of a Fortran program. These results are included in table 2.

For the phosphate-buffered runs, the phosphate concentration was varied, but maintained as low as possible to minimize complexation. The $\log_{10} m_{Ni}$ values showed no enhancement at the higher phosphate concentrations that would have been consistent with the formation of nickel phosphate complexes. The pH_m values in these experiments are sufficiently low as to assure that Ni^{2+} predominates in solution.

The concentration of boric acid was varied by a factor of 7.4 to test for possible complexation of Ni^{2+} by borate. However, the nickel concentrations were far higher than all the remaining data collected in this study and were in the reverse order with respect to boric acid concentration if complexation were the cause of these anomalous results. No explanation for these results can be offered at this time and, therefore, these results were not used further. Interestingly, these boric acid buffer solutions were also used in two low-temperature experiments (see below) and in a companion investigation

Table 3. Summary of results for the solubility of $Ni(OH)_2$(cr) from the low-temperature flow-cell experiments at a flow rate of 0.02 mL m^{-1} (water activities are taken as 1.0000; No sam. refers to the number of samples analyzed; Δtime corresponds to the total duration of each experiment).[a,b]

t (°C)	No. sam.	Δ(time) (h)	Buffer	$m_{buffer} \times 10^{-3}$	$I_m \times 10^{-4}$	pH_m	$\gamma_{\pm(NaCl)}$	$\log_{10} m_{Ni}$	$\log_{10} K^o_{s0}$
25.0	8	233	$B(OH)_3$	2.402	1.3	7.693	0.987	−4.17 ± 0.01	11.28
25.0	12	585	$B(OH)_3$	0.393	0.60	8.235	0.991	−4.56 ± 0.06	11.93

[a,b] See footnotes of table 2.

of cupric oxide solubility where excellent agreement was found with results of other buffered solutions.

3.4. *Low-temperature flow-through cell experiments*

Two sets of experiments were carried out successfully with this apparatus at 25.0°C using boric acid–borate buffered solutions (table 3), whereas three experiments using dilute NaOH feed solutions at 40°C, 60°C, and 75°C failed to produce meaningful results. The difference between the two $\log_{10} K^o_{s0}$ values in table 3 is significantly greater than their combined experimental uncertainties, but they bracket the more numerous HECC values and were retained in the overall fit. Minor contributions from hydrolysis to the second higher pH_m value were ignored here.

3.5. *Discussion solubility constant results*

The $\log_{10} m_{Ni}$ and pH_m values in tables 1–3 were used to calculate $\log_{10} K^o_{s0}$ according to equilibrium (2). The simplest equation that provided the best fit of these data was a weighted linear least-squares regression as shown in equation (13).

$$\log_{10} K^o_{s0} = -(2.710 \pm 0.135) + (4288.48 \pm 44.21)/T. \quad (13)$$

The plot of $\log_{10} K^o_{s0}$ *versus* reciprocal temperature (kelvin) is given in figure 5. As equation (13) dictates, this relationship is clearly linear over the temperature range 0–200°C ($r^2 = 0.9890$) and the values obtained by the two techniques and from the various solid phases are completely concordant with the exception of the results of run 1 that were not included in the fit. The results from the two boric acid buffered experiments at 100°C that are clearly outliers were also not included in the fit.

This agreement, coupled to the number of experiments carried out with the HECC using two different starting acidities and different starting temperatures, which were cycled in different directions, give a high degree of confidence that equilibrium was established in each case. In view of the large discrepancies between virtually all the previous investigations (figure 6), it was deemed very important to establish this fact.

It can also be seen from figure 5 that fits of the solubility constants for NiO(cr) [8] and β-$Ni(OH)_2$(cr) intersect at (351 K, 77°C), which compares exactly (with fortuitous precision) to the value of 77°C calculated for the transition temperature of these two phases from published thermodynamic data (figure 3). These results also show that β-$Ni(OH)_2$(cr) can persist as a meta-stable phase at least up to 200°C and would explain

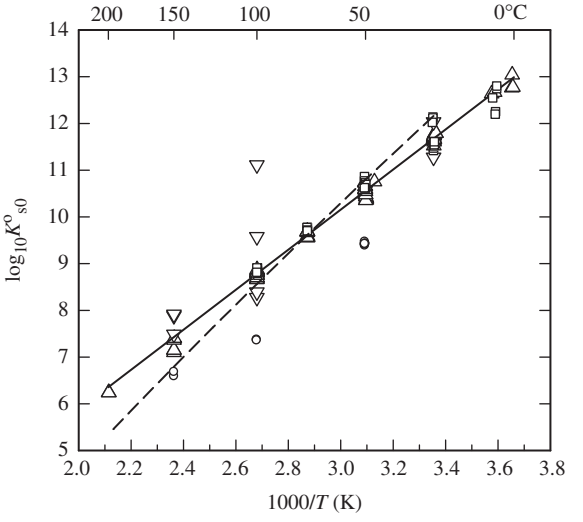

Figure 5. The dependence of $\log_{10} K^{o}_{s0}$ on the reciprocal temperature (kelvin) where the solid line was derived from equation (13) whereas the dashed line represents the corresponding equilibrium for NiO(cr) [8]. The symbols represent: Δ, values obtained using the HECC with β-$Ni(OH)_2$(cr) solids prepared at ORNL; □, values (HECC) using two solid batches supplied by Prof. Gamsjäger; ○, values (HECC) from run 1; ▽, values obtained from the flow-cell experiments.

why Ziemniak *et al*. [4, 6] predicted a much higher transition temperature for the hydration of NiO(cr) based on their relatively short-retention flow-through experiments with NiO(cr) beginning at higher temperatures. From a practical standpoint, consideration of the kinetics of the phase changes for the nickel species during PWR midcycle is an important factor and this observation is consistent with previous work [8, 15].

A comparison of the $\log_{10} K^{o}_{s0}$ values calculated from equation (13) with values taken from the literature is given in figure 6. Of these selected references only Mattigod *et al*. [9] and Gamsjäger *et al*. [5] carried out extensive experimental work on well-characterized solids. In the former study, a large number of individual mixtures of solid and solution were equilibrated (and sampled periodically) at 25°C and pH was measured with a glass electrode. In the more recent study, Gamsjäger and coworkers used a flow-through technique with in-line pH monitoring, again with a cell – Ag | AgCl || solution β-$Ni(OH)_2$ | glass electrode – at temperatures of 35–80°C. In these experiments, the ionic strength was varied from 0.5 to 3.0 mol kg^{-1} ($NaClO_4$) at 50.0°C, whereas at the other temperatures it was maintained at 1.0 mol kg^{-1}.

It is apparent from the data displayed in figure 6 that there is a huge disparity in the solubilities reported over the past 77 years. There is a discernable and expected trend for solid phases referred to in figure 6 as being "freshly prepared" or prepared by "fast precipitation" in that these are expected to be fine-grained, or even amorphous, materials and therefore should exhibit much higher solubilities. Nevertheless, the scatter in the solubility constants at 25°C is almost three orders of magnitude. Many of these reported studies give very little, or no information as to the methods used to characterize their $Ni(OH)_2$ samples. There may also be a question of adequate equilibration times. However, the most likely factors contributing to the large disparity

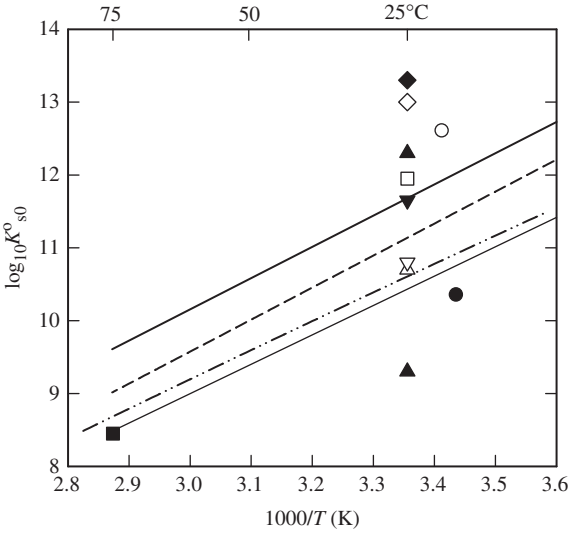

Figure 6. The dependence of $\log_{10} K^{o}_{s0}$ on the reciprocal temperature (kelvin). A comparison with literature data where the solid thick line was derived from equation (13); the dashed line is from [5], the dashed-dot-dot line is from [24] and the thin solid line from the run 1 data; the symbols represent: □ [9]; • [25]; Δ [26]; ▼ [27]; ■ [28]; ▽ [29] aged precipitate; ◆ [29] freshly precipitated; ○ [30]; ◇ [31]; ▲ [32] slowly precipitated.

between these studies are particle size and crystallinity of the $Ni(OH)_2$ solid phase, noting also that measurement of solution pH is rarely described.

4. Particle-size effect on the solubility constant of nickel(II) hydroxide

4.1. *Fractional dissolution*

As mentioned in section 1 an improved method to synthesize β-$Ni(OH)_2$ has been described recently [5, 13]. It is based on the hydrolysis of sodium tetrahydroxonickolate, $Na_2[Ni(OH)_4]$, and leads to pure macrocrystalline nickel(II) hydroxide with crystal sizes up to 0.2 mm. With this coarse crystalline material, solubility equilibria can only be attained from undersaturation, because large crystals of β-$Ni(OH)_2$ will not precipitate in the vicinity of equilibrium within typical experimental time periods. Thus, an invariant solubility constant over a broad range of starting conditions is the criterion for equilibration (pH variation method [33]). Whereas this method has often been successful, it is clearly thermodynamically less rigorous than attaining equilibration from oversaturation and undersaturation. In the present case, the solubility constant obtained for these large crystals was lower by almost one order of magnitude than the one reported by Mattigod *et al.* [9] as illustrated in figure 7(a) and (b).

As this difference exceeds the usual experimental error, the solubility of β-$Ni(OH)_2$(cr) was reinvestigated by the method of fractional dissolution. Batches of synthesized microcrystalline β-$Ni(OH)_2$ were reacted with $HClO_4/NaClO_4$ solutions of constant ionic strength until the pH remained constant. The reaction temperature was kept at 50°C and 80°C, respectively. After metastable or stable solubility

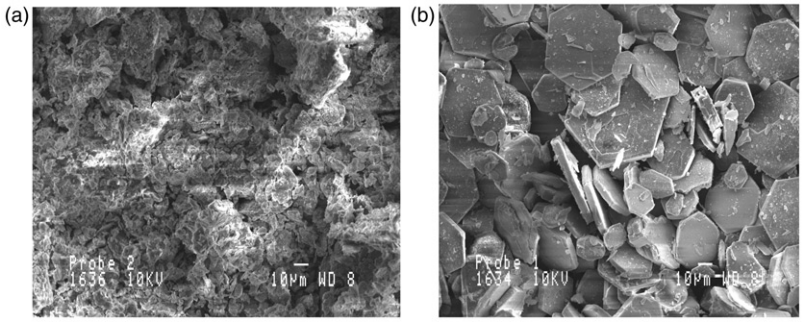

Figure 7. (a) β-Ni(OH)$_2$ precipitated by adding NaOH to 0.2 mol L^{-1} NiCl$_2$ [9], pH $\approx$ 7, $\log_{10} K^{\circ}_{s0} = (11.9 \pm 0.1)$, $I_m = 0$ at 25°C. (b) β-Ni(OH)$_2$ prepared by hydrolysis of Na$_2$[Ni(OH)$_4$] [5] $\log_{10} K^{\circ}_{s0} = (11.03 \pm 0.20)$, $I_m = 0$ at 25°C.

equilibrium (indicated by a constant pH) was attained, the majority of the saturated solution was removed from the reaction vessel, analyzed for Ni(II) and replaced by the same volume of solution. This procedure was repeated until successive final pH values agreed with each other within experimental error limits. The samples were inhomogeneous with respect to the dissolution reaction, but arrived at a stable equilibrium state after the mole fraction of dissolved β-Ni(OH)$_2$(cr) approached 0.25–0.3 (figure 8a and b).

SEM images in figure 9(a) and (b) of samples taken before and after dissolution show that the finely dispersed particles had disappeared.

4.2. *Effect of particle size on solubilities*

Elementary thermodynamic reasoning reveals that the difference in the Gibbs energy of dissolution of finely divided and coarse nickel(II) hydroxide is proportional to the molar surface A_m times surface tension γ [34]. Thus, the logarithmic solubility constant of sparingly soluble metal hydroxides, such as β-Ni(OH)$_2$, is a linear function of the molar surface.

Thermodynamic treatment of the dissolution reaction

$$\beta\text{-Ni(OH)}_2\text{(cr)} \rightleftarrows \text{Ni}^{2+} + 2\text{OH}^- \tag{14}$$

leads to equations (15)–(17),

$$\Delta_{r(x)}G^{\circ}[\beta\text{-Ni(OH)}_2(s, A_m)] - \Delta_{r(x)}G^{\circ}[\beta\text{-Ni(OH)}_2(s, A_m \rightarrow 0)] = (2/3)A_m\sigma, \tag{15}$$

$$A_m = M\alpha/(dp), \tag{16}$$

$$\ln Qs_0(A_m) = \ln Q_{s0}(A_m \rightarrow 0) + (2/3)A_m\sigma/RT, \tag{17}$$

where A_m, σ, M, d, ρ, and α are the molar surface, surface tension, molar mass, particle size, density, and an arbitrary geometric factor, respectively, and $A_m \rightarrow 0$ refers to coarse crystalline material.

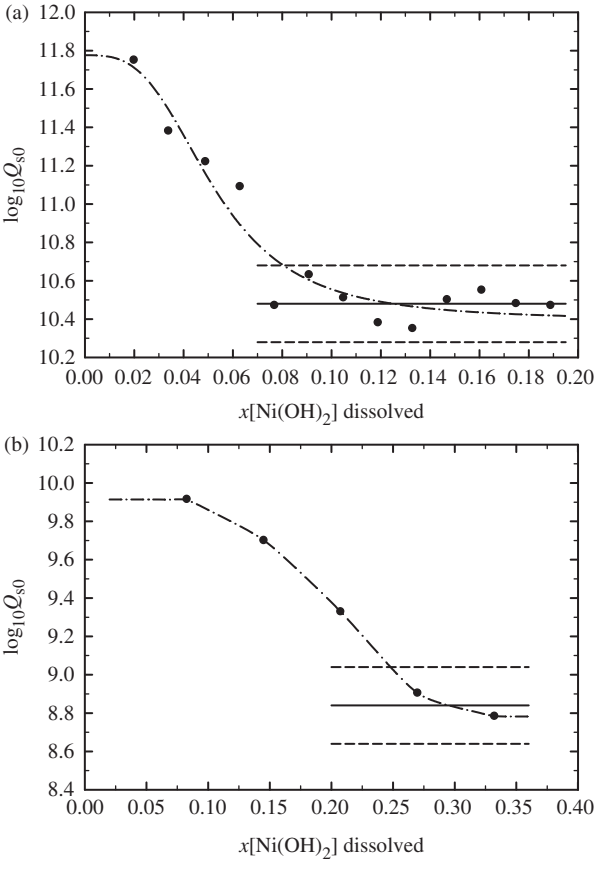

Figure 8. (a) Fractional dissolution of β-Ni(OH)$_2$ (Johnson & Matthey) at 50.0°C, $I_m = 1.00$ ($NaClO_4$), $m_{H^+} = 0.01$ where the solid line represents a mean value of $\log_{10}Q_{s0} = (10.48 \pm 0.20)$. (b) Fractional dissolution of β-Ni(OH)$_2$ (Johnson & Matthey) at 80.0°C, $I_m = 1.00$ ($NaClO_4$), $m_{H^+} = 0.01$ where the solid line represents a mean value of $\log_{10}Q_{s0} = (8.84 \pm 0.20)$.

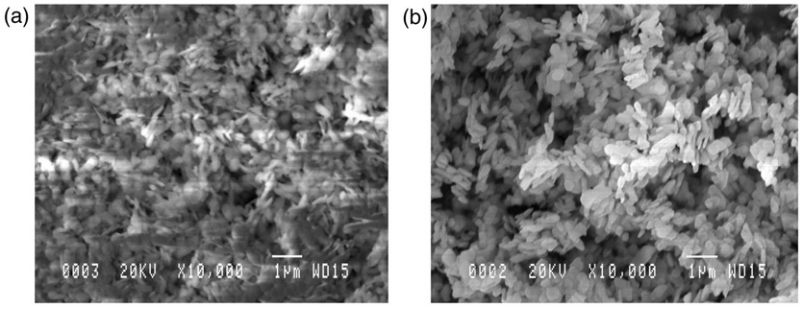

Figure 9. (a) SEM image of the sample before dissolution. (b) SEM image of the sample after dissolution.

Table 4. Estimated molar surface areas of equilibrated β-$Ni(OH)_2$ dissolution fractions.

50.0°C		80.0°C	
$\Delta \log_{10} K_{s0}$ ± 0.2	$A_m/m^2\,mol^{-1}$ ± 4000	$\Delta \log_{10} K_{s0}$ ± 0.2	$A_m/m^2\,mol^{-1}$ ± 4000
1.28	24,000	1.07	22,000
0.91	17,000	0.86	17,000
0.75	14,000	0.49	9900
0.62	11,000		

4.3. *Semi-theoretical estimation of surface tension*

In order to estimate the molar surface of the various β-$Ni(OH)_2$ fractions, information on the surface tension is required (table 4). The semi-theoretical estimation of the molar surface proposed by Schindler *et al.* [35] was applied:

$$A_m = (3/2)RT[\ln Q_{s0}(A_m) - \ln Q_{s0}(A_m \to 0)]/\sigma. \tag{18}$$

Reversible pulverization leads to:

$$-RTlnQ_{s0}(A_m \to 0) = (2/3)\sigma A_m, \tag{19}$$

$$4\pi L[r^2(Ni^{2+}) + 2r^2(OH^-)] = A_m, \tag{20}$$

$$\begin{aligned} &\sigma = 1.5RT \ln Q_{s0}(A_m \to 0)/\{4\pi L[r^2(Ni^{2+}) + 2r^2(OH^-)]\}, \\ &\sigma = (0.50 \pm 0.05)\,J\,m^{-2}. \end{aligned} \tag{21}$$

Numerical values of A_m thus obtained are comparable with those estimated from the particle sizes of Sorai *et al.*'s [36] nickel hydroxide samples. The semi-theoretically derived surface tension γ values of β-$Ni(OH)_2$(cr) lead to reasonable estimates of molar surfaces A_m. At $A_m \approx 1000\,m^2\,mol^{-1}$ measured $Q_{s0}(A_m)$ values become indistinguishable. The same equilibrium value from oversaturation and undersaturation can probably be obtained only when the sizes of dissolving and precipitating particles are similar. The difficulty in measuring reproducible values for $\log_{10} Q_{s0}$ of microcrystalline β-$Ni(OH)_2$ seems quite plausible in light of Oswald and Asper's [37] observation that a specific kinetic hindrance prevents recrystallization of $Ni(OH)_2$ in aqueous media. The solubility of β-$Ni(OH)_2$(cr) is determined by the smallest particles present. The bottom line of this consideration is that thermodynamic data derived from solubility measurements on nickel(II) hydroxide have to be considered with care.

5. Conclusions

Equation (13) represents the consensus of solubility constant data for β-$Ni(OH)_2$(cr) gathered using two completely independent techniques, and multiple solid-phase samples and solution compositions obtained during different temperature

cycling programs. However, there remains the question of the effect of particle size which appears to extend to larger size crystals than is usually observed for metal oxide/hydroxides. Typically, crystals with cross sections >1 μm show consistent solubilities, as is the case for NiO(cr), for example. One explanation for this behavior could lie in the fact that the smaller plate-like hexagonal β-Ni(OH)$_2$ crystals would have a higher percentage of thin edge sites which could exhibit higher dissolution rates accounting for their higher apparent solubility constants. This phenomenon presents an interesting topic for future research coupling kinetic and thermodynamic effects.

Acknowledgments

Much of the experimental work reported here was sponsored by the U.S. Department of Energy under the NEPO initiative in collaboration with EPRI, Inc., Palo Alto, California with project managers Paul Frattini and Keith Frazzetti. Special thanks are also given to Lawrence M. Anovitz for his advice and role in characterizing the nickel hydroxide phases.

References

[1] P. Kritzer, N. Boukis, E. Dinjus. *J. Supercrit. Fluids*, **15**, 205 (1999).
[2] D.D. Macdonald, G.A. Cragnolino. In *The ASME Handbook on Water Technology for Thermal Power Plants*, Chapter 9, P. Cohen (Ed.), EPRI Project No. RP 1958-1, pp. 701–712, The American Society of Mechanical Engineers (1989).
[3] D.J. Wesolowski, S.E. Ziemniak, L.M. Anovitz, M.L. Machesky, P. Bénézeth, D.A. Palmer. In *Aqueous Systems at Elevated Temperatures and Pressures: Physical Chemistry in Water, Steam and Hydrothermal Solutions*, D.A. Palmer, R. Fernández-Prini, A.H. Harvey (Eds.), Chapter 14, pp. 493–595, Elsevier/Academic Press, Amsterdam, New York, (2004).
[4] S.E. Ziemniak, M.E. Jones, K.E.S. Combs. *J. Solution Chem.*, **18**, 1133 (1989).
[5] H. Gamsjäger, H. Wallner, W. Preis. *Monatsh. Chem.*, **133**, 225 (2002).
[6] S.E. Ziemniak, M.A. Goyette. *J. Solution Chem.*, **33**, 1135 (2004).
[7] D.D. Wagman, W.H. Evans, V.B. Parker, R.H. Schumm, I. Halow, S.M. Bailey, K.L. Churney, R.L. Nuttall. *J. Phys. Chem. Ref. Data*, **11**, 2–38, 2–166 (1982).
[8] P.R. Tremaine, J.C. LeBlanc. *J. Chem. Thermodyn.*, **12**, 521 (1980).
[9] S.V. Mattigod, D. Rai, A.R. Felmy, L. Rao. *J. Solution Chem.*, **26**, 391 (1997).
[10] D.A. Palmer, P. Bénézeth, D.J. Wesolowski. *Geochim. Cosmochim. Acta*, **65**, 2081 (2001).
[11] C.F. Baes Jr, R.E. Mesmer. *The Hydrolysis of Cations*, p. 246, John Wiley and Sons, New York (1976).
[12] P. Bénézeth, D.A. Palmer, D.J. Wesolowski, C. Xiao. *J. Solution Chem.*, **31**, 947 (2002).
[13] H. Wallner, K. Gatterer. *Z. Anorg. Allg. Chem.*, **628**, 2818 (2002).
[14] T. Mukaibo, M. Masukawa, M. Maeda, M. Hoshido. *Denki-Kagaku*, **34**, 388 (1966).
[15] T.W. Swaddle, T.C.T. Wong. *Can. J. Chem.*, **56**, 363 (1978).
[16] J.R. Taylor, A.T. Dinsdale. *Z. Metallkd.*, **81**, 354 (1990).
[17] I. Ansara, B. Sundman. In *Computer Handling and Dissemination of Data*, P.S. Glaeser (Ed.), pp. 154–158, Elsevier Science Publishers, New York (1987).
[18] H. Gamsjäger, J. Bugajski, T. Gajda, R.J. Lemire, W. Preis. *Chemical Thermodynamics of Nickel*, F. Mompean, M. Illemasséne, J. Perrone (Eds.), Elsevier, Amsterdam (2005).
[19] W.T. Lindsay Jr. In *The ASME Handbook on Water Technology for Thermal Power Plants*, P. Cohen, (Ed.), Chapter 7, p. 483, The American Society of Mechanical Engineers, USA (1989).
[20] D.G. Archer. *J. Phys. Ref. Data*, **21**, 793 (1992).
[21] R.E. Mesmer, C.F. Baes Jr. *J. Solution Chem.*, **3**, 307 (1974).
[22] D.A. Palmer, P. Bénézeth, D.J. Wesolowski. *PowerPlant Chem.*, **2**, 261 (2000).
[23] W.L. Marshall, E.U. Franck. *J. Phys. Chem. Ref. Data*, **10**, 295 (1981).
[24] N.V. Plyasunova, Y. Zhang, M. Muhammed. *Hydrometallurgy*, **48**, 43 (1998).

[25] H.T.S. Britton. *J. Chem. Soc*., 2110 (1925).
[26] K.H. Gayer, A.B. Garrett. *J. Am. Chem. Soc*., **71**, 2973 (1949).
[27] G.M. Schwab, K. Polydoropoulos. *Z. Anorg. Allg. Chem*., **274**, 234 (1953).
[28] G.N. Dobrokhotov. *Zh. Prikl. Khim*., **76**, 1056 (1954).
[29] W. Feitknecht, W. Hartmann. *Chimia*, **8**, 95 (1954).
[30] F. Guta, Z. Ksandr, M. Hejtmánek. *Coll. Czech. Chem. Commun*., **21**, 1388 (1956).
[31] T. Kawai, H. Otsuka, H. Ohtaki. *Bull. Chem. Soc. Japan*, **46**, 3753 (1973).
[32] D.M. Novak-Adanić, B. Ćosović, H. Bilinski, M. Branica. *J. Inorg. Nucl. Chem*., **21**, 1388 (1956).
[33] P. Schindler. *Chimia*, **17**, 313 (1963).
[34] B.V. Enüstün, J. Turkevich. *J. Am. Chem. Soc*., **82**, 4502 (1960).
[35] P.W. Schindler. *Adv. Chem. Ser*., **67**, 196 (1967).
[36] M. Sorai, A. Kosaki, H. Suga, S. Seki. *J. Chem. Thermodyn*., **1**, 119 (1969).
[37] H.R. Oswald, R. Asper. In *Preparation and Crystal Growth of Material with Layered Structures*, R.M.A. Lieth (Ed.), pp. 71–140, Reidel, Dordrecht-Holland (1977).